ACS APPLIED MATERIALS & INTERFACES

Research Article

www.acsami.org

Nanoporous Bicontinuous Structures via Addition of Thermally-Stable Amphiphilic Nanoparticles within Block Copolymer Templates

Seyong Kim,[†] Misang Yoo,[†] Nana Kang,[‡] Bongjin Moon,[‡] Bumjoon J. Kim,[§] Soo-Hyung Choi,[∥] Jaeup U. Kim,[⊥] and Joona Bang*[,†]

[†]Department of Chemical and Biological Engineering, Korea University, Seoul 136-701, Republic of Korea

[‡]Department of Chemistry, Sogang University, Seoul 121-742, Republic of Korea

[§]Department of Chemical and Biomolecular Engineering, Korea Advanced Institute of Science and Technology, Daejeon 305-701, Republic of Korea

[∥]Department of Chemical Engineering, Hongik University, Seoul 121-791, Republic of Korea

[⊥]School of Mechanical and Advanced Materials Engineering, UNIST, Ulsan 689-805, Republic of Korea

Supporting Information

ABSTRACT: Herein, we fabricated the bicontinuous structures from nanocomposites of poly(styrene-*b*-methyl methacrylate) (PS-*b*-PMMA) block copolymer and the shell-cross-linked, thermally stable gold nanoparticles (Au NPs). The surface property of Au NPs was controlled with ligands containing various compositions of PS and PMMA so that the resulting Au NPs were selective to PS or PMMA block or nonselective (i.e., neutral) to both blocks. The amphiphilic Au NPs were also prepared by coating the surface of Au NPs with equimolar mixtures of PS and PMMA selective ligands. Consequently, it was found that the morphological behaviors of thermally annealed nanocomposites containing amphiphilic Au NPs and PS-*b*-PMMA were dramatically different from the case of neutral Au NPs that were coated with nonselective ligands. With increasing the amount of amphiphilic Au NPs, a transition from lamellar to bicontinuous structures was observed, whereas the neutral Au NPs were aggregated within the PS-*b*-PMMA lamellae. Furthermore, the nanoporous bicontinuous thin films were fabricated on the silicon substrates and the morphological behaviors were quantitatively investigated by grazing-incidence small-angle X-ray scattering (GISAXS) analysis.

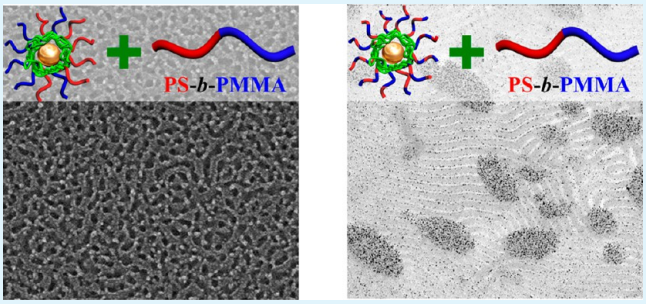

KEYWORDS: *Au nanoparticles, thermal stability, block copolymer, bicontinuous structure*

INTRODUCTION

Nanocomposite materials composed of metal or inorganic nanoparticles (NPs) dispersed in polymer matrices have been widely investigated because of improved electrical and thermal conductivity, mechanical strength, and optical and magnetic properties. These materials are potentially applicable to photonic band gap materials, sensors, memory devices, and electronics.[1−10] In practice, NPs are mediated by organic or polymeric ligands to acquire the enhanced compatibility with polymer matrices and, therefore, a well dispersed system without aggregation of NPs. Here, fine-tuning of surface property with a judicious selection of ligands including small molecules, homopolymers, and copolymers provides successful control of positioning NPs in the polymer matrices with multiple domains.[8,11−23] However, these nanocomposite materials typically suffered from desorption of ligands from the NPs at elevated temperature, resulting in macrophase separation, and diminished merit of blending.[24] Recently, thermal stability of NPs has been achieved by cross-linking the ligands surrounding NPs, which enables us to use facile material process (i.e, thermal annealing) without considering complicated interactions induced by solvents.[25−29]

Furthermore, recent studies showed that the use of the interfacially active NPs provides new strategies to control the morphology of block copolymer and the orientation of block copolymer thin film by alleviating the interfacial tension.[17−19,30−32] Particularly, Kim et al. reported a morphological transition from lamellae to bicontinuous morphology by introducing Au NPs coated with polystyrene (PS) into poly(styrene-*b*-2-vinylpyridine) (PS-*b*-P2VP) block copolymer, in which the favorable interaction between P2VP and Au provides strong interfacially active property.[17−19,30] And, Jang et al. also produced bicontinuous morphology of PS-*b*-P2VP created by thermally stable Au−Pt NPs.[28] Such phase transition from lamellae to bicontinuous structures were predicted by Pryamitsyn and Ganesan that the segregation of nanoparticles to the interface leads to a decrease in interfacial tension and a

Received: March 18, 2013
Accepted: May 29, 2013
Published: May 29, 2013

corresponding decrease in the lamellar thickness. As a consequence, the bending modulus of the lamellae decreases and it produces an instability that ultimately results in the formation of bicontinuous structures.[33] In parallel, Yoo et al. observed that the orientation of poly(styrene-*b*-methyl methacrylate) (PS-*b*-PMMA) block copolymer thin film can be controlled by thermally stable Au NPs that are either selective to PMMA or neutral to PS and PMMA domains.[31]

In this study, we report the synthesis of thermally stable and interfacially active amphiphilic Au NPs, and their use for creating bicontinuous PS-*b*-PMMA morphology. Amphiphilic Au NPs were prepared by coating a mixture of two different thiol-terminated PS and PMMA selective ligands on Au NPs using a similar method as reported by Kim et al.[19] Then, photocross-linking by UV light was performed to endow amphiphilic Au NPs with excellent thermal stability. Incorporation of the amphiphilic Au NPs into lamellar forming PS-*b*-PMMA thin film provides transition in orientation from parallel to perpendicular lamellae at low NP volume fraction (ϕ_{NP} < 5%), and transition from lamellae to bicontinuous morphology at higher ϕ_{NP}. In comparison, Au NPs coated with nonselective ligands in PS-*b*-PMMA matrix showed macrophase separation at ϕ_{NP} > 8%, which suggests that the amphiphilic Au NPs are interfacially more active and highly adsorbed at the interface. This transition has been observed by transmission electron microscopy (TEM) and grazing-incidence small-angle X-ray scattering (GISAXS) in combination with detailed fitting model.

EXPERIMENTAL SECTION

Synthesis of Polymeric Ligands. The thiol-terminated polymeric ligands were synthesized by reversible addition−fragmentation transfer (RAFT) polymerization as described previously.[26,31] For P[(MMA-*r*-S)-*b*-P(S-N_3)]-SH (ligand-1 and ligand-2), mixtures of methyl methacrylate (MMA), styrene, RAFT agent, and 2,2′-azobis-(isobutyronitrile) (AIBN) were purged with nitrogen gas in a Schlenk flask, and then polymerized at 70 °C for 6 h to produce P(MMA-*r*-S)-RAFT after precipitating into methanol. The molar feed ratios of MMA and styrene were 8:2 and 2:8 for ligand-1 and ligand-2, respectively. The molecular weights (M_n values) of P(MMA-*r*-S)-RAFT were 2300 and 2100 g/mol for ligand-1 and ligand-2, respectively. For the second block, P(MMA-*r*-S)-RAFT, 4-vinylbenzyl chloride (S−Cl), and AIBN were mixed and purged with nitrogen gas, and then polymerized at 70 °C for 10 h to produce P[(MMA-*r*-S)-*b*−S-Cl]. The total M_n values and polydispersity index (PDI) of P[(MMA-*r*-S)-*b*-S-Cl] were 3000 g/mol and 1.19 for ligand-1 and 2800 g/mol and 1.20 for ligand-2, respectively. The P[(MMA-*r*-S)-*b*-S-Cl] was then dissolved in dry THF with hexylamine and purged with nitrogen gas. The substitution reaction was performed at room temperature overnight. The mixture was precipitated into methanol to produce thiol-terminated P[(MMA-*r*-S)-*b*-S-Cl]-SH as a white solid powder. The polymer was then mixed with 4 equivalents of sodium azide in dimethylformamide under ambient conditions for 24 h. The resulting P[(MMA-*r*-S)-*b*-S-N_3]-SH was precipitated into methanol and dried in vacuo. The other ligand, P[S-*b*-P(S-*r*-S-N_3)]-SH (ligand-3), was synthesized using the same procedure described above, but the first block was polymerized with styrene only, and the second block was copolymerized with styrene and S−Cl with the feed mole ratio of 7:3.

Synthesis of Thermally Stable Gold Nanoparticles. The synthesis of Au NPs coated with these ligands was accomplished using the two-phase method. The mole feed ratio of the polymer ligand to Au atoms was 0.3. For the amphiphilic Au NPs, the equimolar ratio of ligand-1 and ligand-3 were used. The resulting Au NPs were separated from unattached polymer and residues by ultrafiltration membrane (MWCO 30 000 Da, Millipore, Inc.) using dimethylformamide (DMF) as a solvent several times. To impart thermal stability via cross-linking, the Au NPs were dispersed in dioxane and the solutions were exposed to the UV light (λ = 254 nm) for 1 h under ambient conditions using a hand UV lamp (intensity of ∼2 mW/m^2). The cross-linked Au NPs were separated by centrifugation and dried in vacuo overnight.

Preparation of Nanocomposite Bulk and Thin Films. A 2 wt % dichloromethane solution of lamellar forming PS-*b*-PMMA block copolymer (M_n = 187 kg/mol and PDI = 1.10, Polymer Source, Inc.) was mixed with 10 wt % of cross-linked Au NPs relative to the polymer. To compare the morphological behaviors between neutral-ligand Au NPs and mixed-ligand Au NPs, the weight fractions were varied from 10 to 60 wt %. The nanocomposite samples were prepared by drop casting the solution on the NaCl substrates and thermally annealed at 200 °C for 48 h. The volume fraction (ϕ_{NP}) of Au NPs in the nanocomposites was estimated from the density of polymer (∼1.05 g/mol) and Au (∼19.3 g/mol) and by thermal gravimetric analysis (TGA) of the Au NPs. The weight fractions of neutral-ligand Au NPs, 5, 10, 20, 30, 40, 50, and 60 wt % correspond to 2.0, 4.1, 8.2, 12.3, 16.4, 20.5, and 24.6 vol %, respectively, and the weight fractions of mixed-ligand Au NPs, 5, 10, 20, 30, 40, 50, and 60 wt % correspond to 2.1, 4.2, 8.4, 12.6, 16.8, 21.0, and 25.3 vol %, respectively.

For the fabrication of nanoporous bicontinuous thin films, two symmetric PS-*b*-PMMA block copolymers (M_n = 130 kg/mol and PDI = 1.09, M_n = 187 kg/mol and PDI = 1.10, Polymer Source, Inc.) were mixed with mixed-ligand Au NPs in toluene. A weight fraction of NPs was varied from 10 to 60 wt % relative to the block copolymers, keeping the total concentration of 2.5 wt %. The nanocomposite thin films were spin coated from the toluene solution onto silicon substrates without a neutral layer, resulting in thin films with thickness of ∼200 nm. The thin films were annealed at 200 °C for two days in a vacuum.

Characterization. The size of Au NPs and the location of these NPs in the block copolymer matrix were examined by transmission electron microscopy (TEM), a Tecnai 20 electron microscope operating at 200 kV. The Au NPs were dissolved at a very low concentration in dichloromethane or acetone. A drop of these solutions was placed onto carbon film-coated TEM grids and dried in air. To obtain cross-sectional TEM images of nanocomposites in the bulk state, the annealed samples were floated by removing the NaCl substrate on DI water and then transferred to an epoxy support. Embedded films were microtomed into a section several tens of nanometers thick. PS domains were stained with ruthenium tetroxide (RuO_4), which selectively stained the PS domains.

For the analysis of nanocomposite thin films, the films were irradiated by UV light with a wavelength of 254 nm at a dose of 25 J/cm^2 (XX-15S; UVP Inc.) under vacuum for 10 min, rinsed in acetic acid, and then rinsed in water to completely cleave the PMMA block. The resulting nanoporous thin films were examined by field emission scanning electron microscope (FE-SEM). The nanocomposite thin films were also examined by grazing-incidence small-angle X-ray scattering (GISAXS) that was measured at the 9A beamline at the Pohang Accelerator Laboratory (PAL), Korea. 2D GISAXS patterns were recorded using a CCD detector positioned at the end of a vacuum guide tube when the X-rays pass through the BCP thin films under vacuum, where the operating conditions were set to a wavelength of 1.38 Å and a sample-to-detector distance of 2.2 m. In the scattering geometry, q_y is the scattering vector normal to the plane of incidence (parallel to the film surface), where the domain spacing is determined by $L_o = 2\pi/q_y^*$, where L_o corresponds to the domain spacing of lamellae. q_z is the scattering vector normal to the sample surface, defined as $q_z = (4\pi/\lambda)\sin\theta$, where λ is the wavelength of the X-rays and 2θ is the scattering angle. The incident angle was set at 0.18°, which is above the critical angle (0.135°) for PS-*b*-PMMA thin films.

RESULTS AND DISCUSSION

As we demonstrated previously, the surface property of thermally stable Au NPs can be adjusted by varying the

Scheme 1. Schematic Illustration for the Synthesis of (a) P[(S-*r*-MMA)-*b*-S-N_3]-SH and (b) P[S-*b*-(S-*r*-PS-N_3)]-SH

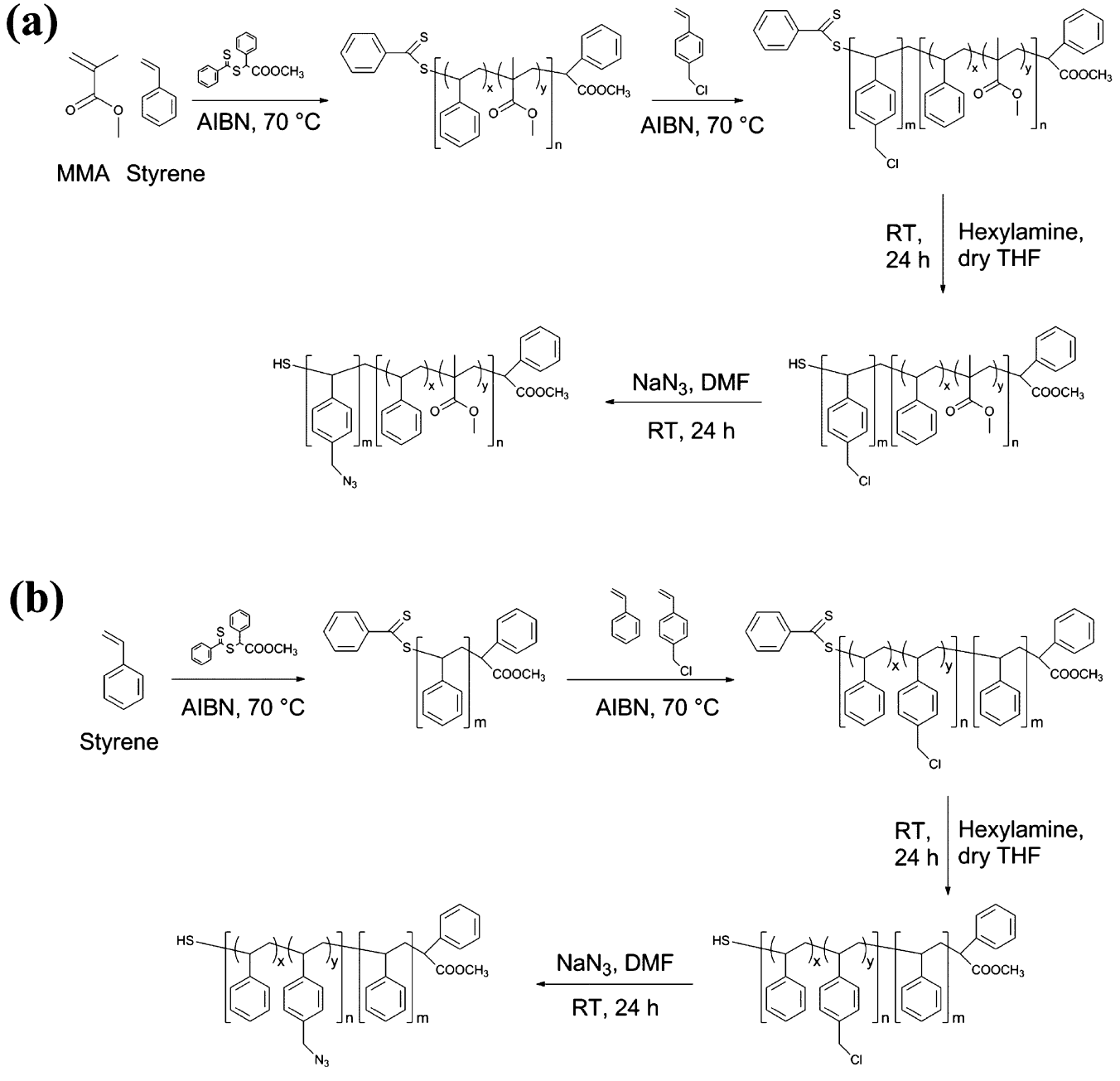

composition of thiol-terminated polymeric ligands, and the location of Au NPs within block copolymer templates can be controlled.[31] In a similar manner, herein we synthesized three different ligands via RAFT polymerization as described in Scheme 1, and they were used to prepare the Au NPs that are selective to either PS or PMMA block or neutral to both blocks. For PMMA-selective and neutral Au NPs, the ligands were designed as P[(MMA-*r*-S)-*b*-S-N_3]-SH, where the composition of PMMA and PS in the brush part, P(MMA-*r*-S) block, were adjusted as 80:20 and 20:80 for PMMA selective and neutral Au NPs, respectively, and they are denoted as ligand-1 and ligand-2, respectively. It should be noted that the pure PMMA brush was not considered for PMMA selective Au NPs, because the second P(S−N_3) block is not readily added to the PMMA-RAFT, and the pure PMMA block can be degraded during UV cross-linking of the P(S−N_3) shells. Also, the neutral composition of P(MMA-*r*-S) brush was found as 20:80, not ∼40:60 (neutral composition of P(MMA-*r*-S) in the flat surface for the block copolymer patterns) because of the presence of polar, inner P(S-N_3) shell containing the nitrogens in azidirine or diazo moieties.[26,31] For PS-selective Au NPs, it was found that the polarity of inner shell needs to be minimized, while keeping the minimum amount of azido groups for UV cross-linking. In this case, the optimal composition of P(S-N_3) block in the inner block was found to be ∼30% for the PS selective ligand, P[S-*b*-P(S-*r*-S-N_3)]-SH, denoted as ligand-3. As summarized in Table 1, the molecular weight (M_n) of the brush, either P(MMA-*r*-S) or PS block, was controlled as 1900−2300 g/mol, and the M_n of the shell block, either P(S-N_3) or P(S-*r*-S-N_3), was adjusted as 700−1000 g/mol, leading to the total M_n of ligands as 2800−3000 g/mol with the narrow polydispersity index (PDI).

dx.doi.org/10.1021/am400999z | ACS Appl. Mater. Interfaces 2013, 5, 5659−5666

Table 1. List of the Synthesized Polymeric Ligands

ligands	brush Mn (g/mol)	total Mn (g/mol)	feed mole ratio of PMMA/PS in brush	feed mole ratio of PS-N_3/PS in shell	PDI
P[(MMA-r-S)-*b*-P(S-N_3)]-SH (ligand-1)	2300	3000	80: 20	100:0	1.19
P[(MMA-r-S)-*b*-P(S-N_3)]-SH (ligand-2)	2100	2800	20: 80	100:0	1.20
P[S-*b*-P(S-r-S-N_3)]-SH (ligand-3)	1900	2900	0:100	30:70	1.18

These ligands were used to synthesize the polymer coated Au NPs via two phase method.[17,18] The ungrafted ligands and residual reagents were removed by washing with a good solvent, dimethylformamide using an ultrafiltration membrane. Then, they were dispersed in dioxane that is UV transparent, and irradiated with UV light for ∼1 h to cross-link the P(S-N_3) or P(S-*r*-S-N_3) shell. The core diameters of resulting Au NPs were <3 nm (see Supporting Information, Figure S1). To examine the location of Au NPs within the block copolymer templates, the nanocomposite samples were prepared by adding 10 wt % of Au NPs to the lamellar forming PS-*b*-PMMA block copolymer with M_n = 187 kg/mol (PS volume fraction, f_{PS} = 0.516) and PDI = 1.10. From the TEM images in Figure 1, Au NPs coated with ligand-1 (PMMA rich) and ligand-3 (PS rich) were located within PMMA and PS domain, respectively, as expected from the composition of ligands, and thus they are denoted as PMMA-Au NPs and PS-Au NPs, respectively. For Au NPs coated with ligand-2 that has the neutral composition of PS and PMMA, it was observed that they were clearly localized at the interface of PS and PMMA domain (denote as neutral-ligand Au NPs).

The surface property of Au NPs can be precisely tuned by coating Au NPs with a mixture of two different polymer ligands, their random copolymers, or homopolymers with controlled areal chain density.[17,18] While all of the above approaches can produce interfacially active Au NPs for block copolymer matrix, each different method can produce different local distribution of the polymers on the Au NPs, which eventually determines the magnitude of the interfacial activity of the Au NPs. For example, Kim et al. found that the Au NPs coated with a mixture of PS and P2VP ligands exhibited much stronger adsorption behavior to the PS/P2VP interface compared to the case of PS-*r*-P2VP coated Au NPs due to the redistribution of PS and P2VP homopolymers on the Au surface to form the amphiphilic, Janus NPs.[18] In addition, it was demonstrated that the PS coated Au NPs with reduced chain areal density could behave as NP surfactant in PS-*b*-P2VP matrix due to very strong interfacial activity, produced by the combination of redistribution of PS chains on Au NPs and strong favorable attraction of bare Au surface with the P2VP block.[19] Therefore, these Au NPs could induce the morphological transition from lamellae to bicontinuous structures. As these examples were demonstrated under the solvent annealing conditions due to the thermal instability of traditional ligands coated Au NPs, this strategy was recently extended to the thermally stable NPs, consisting of Au core and Pt shell with PS brushes, showing a transition from a lamellar to bicontinuous morphology via thermal annealing.[28] In both cases, the formation of bicontinuous structure is attributed to the strong adsorption of Janus Au NPs to the PS/P2VP interfaces.

To further explore the effect of surface property of Au NPs on the morphologies of block copolymer nanocomposites, we prepared the Au NPs by mixing ligand-1 (PMMA selective) and ligand-3 (PS selective) in equimolar ratio, denote as mixed-ligand Au NPs. From the proton NMR, we estimated an actual molar ratio of ligands on Au NPs and it corresponds to 0.56:

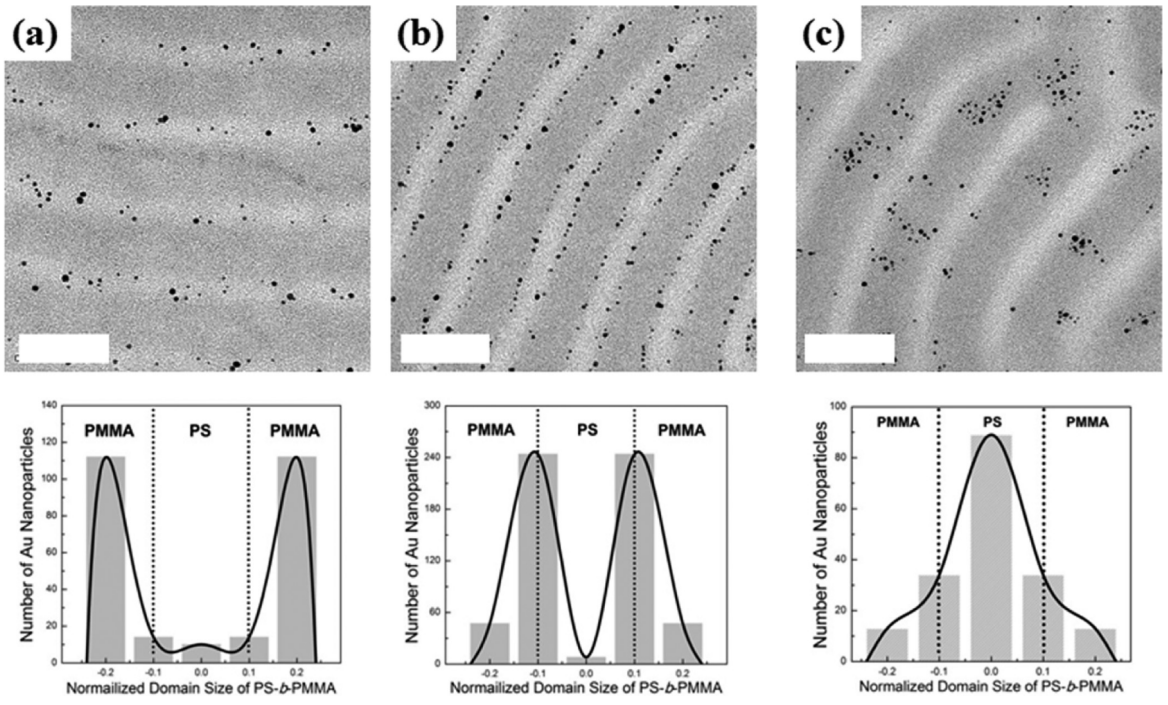

Figure 1. Cross-sectional TEM images and the corresponding histogram for the location of 10 wt % Au NPs coated with (a) ligand-1 (PMMA selective), (b) ligand-2 (neutral), and (c) ligand-3 (PS selective) within PS-*b*-PMMA block copolymer (M_n = 187 kg/mol). Scale bars are 100 nm.

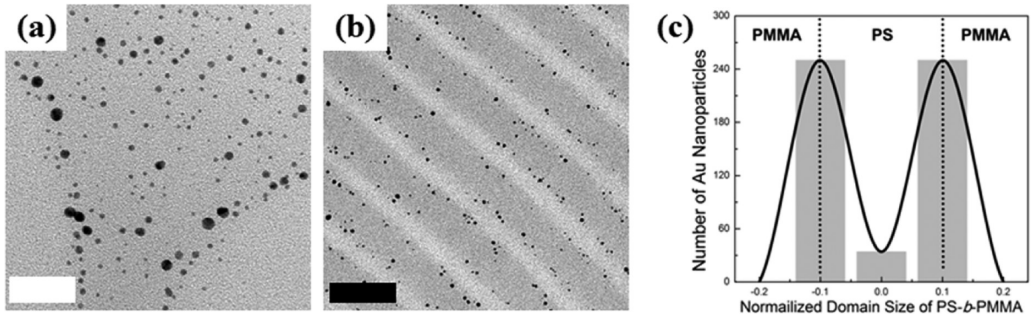

Figure 2. (a) TEM image of as synthesized mixed-ligand Au NPs. The measured diameter of Au core is 2.92 ± 1.00 nm. (b) Cross-sectional TEM image and (c) the corresponding histogram for the location of 10 wt % mixed-ligand Au NPs within PS-*b*-PMMA (M_n = 187 kg/mol). White scale bar in panel a is 40 nm, and the black scale bar in panel b is 100 nm.

0.44 for ligand-1: ligand-3, which is not very different from the feed mole ratio. When 10 wt % (volume fraction, ϕ_{NP} = 4.2%) of mixed-ligand Au NPs were added to 187 kg/mol PS-*b*-PMMA block copolymer, it was observed that Au NPs were clearly localized at the PS/PMMA interface (Figure 2) as with the case of neutral-ligand Au NPs, indicating that they also exhibit the amphiphilic surface property. It is known that mobile PS and PMMA ligands on Au NPs can be redistributed to produce 2-D phase separation of the polymers on the surface of Au NPs.[13,18,34] In the case of uncross-linked Au NPs that were coated with PS and P2VP ligands, Kim et al. estimated $N\chi$ as ∼2.6 for 1,500 g/mol ligands, which is only moderately above the critical value $N\chi$ = 2 for phase separation.[18] Therefore, the possibility for spontaneous phase separation of ligands on Au NPs in the solution may be excluded. Instead, they suggested that PS and P2VP ligands can redistribute on the Au surface once the particle is in contact with high molecular weight PS-*b*-P2VP block copolymer at the interface. In our system, the $N\chi$ value is only ∼1.2, assuming 3000 g/mol of PS and PMMA ligands, and it is certainly lower than the critical value $N\chi$ = 2 for phase separation. Therefore, we also conjecture that the ligands can be segregated after incorporation of Au NPs within PS-*b*-PMMA block copolymer templates. In our system, although the mobility of polymeric ligands on the Au NP surface might be rather limited because of the cross-linked inner shell of polymer ligands, some degree of phase separation can be still expected due to mobile upper brush part of ligands that are significantly longer than the inner shell. Therefore, we suggest that they can rearrange by interaction with the high molecular weight PS-*b*-PMMA chains, thereby leading to phase separation of brushes on the Au NP and providing strong adsorption energy of the Au NPs to the PS/PMMA interface.[35] As to experimental technique to confirm the Janus-type distribution of ligands on Au NPs, Stellacci and co-workers recently employed the 2D-NOESY-NMR technique to scrutinize the ligand distribution on the Au NPs that were coated with two kinds of small molecules, aliphatic and aromatic ligands.[36] In this case, the Janus distribution of ligands was confirmed by the absence of cross-peaks, as the cross-peaks indicate that the distance between two ligands is less than 0.4 nm. We also performed a 2D-NOESY-NMR experiment for the Au NPs coated with ligand-1 and ligand-3 mixture, and it was observed that the cross-peaks are not present (data not shown). This may suggest the possibility that ligands were segregated on the Au NPs, but we think that the case is different in our system. Since we employed the polymeric ligands with molecular weight of ∼3000 g/mol, it can be expected that these ligands are not closely packed within <0.4 nm as with small ligands used by Stellacci and co-workers. Therefore, although the absence of the cross-peaks does not exclude the possibility of Janus-type distribution of ligands, we would not like to conclude the 2D-NOESY-NMR results as a confirmation of Janus-type distribution of polymeric ligands in our system. Alternatively, we plan to characterize the distribution of polymeric ligands in our system by small angle neutron scattering (SANS), as Lang and co-workers suggested by simulation that the form factors from Janus particles and homogeneous core−shell particles can be distinguished if the contrast can be varied.[37]

The morphologies of nanocomposites containing various contents of neutral- and mixed-ligand Au NPs within PS-*b*-PMMA block copolymer were investigated as shown in Figures 3 and 4. With increasing the volume fraction (ϕ_{NP}) of neutral-ligand Au NPs from ∼8 vol % to ∼21 vol %, the region of aggregated Au NPs can be clearly seen whereas the other Au NPs are localized at the PS/PMMA interface. In this case, it should be noted that the lamellae structures preserve regardless

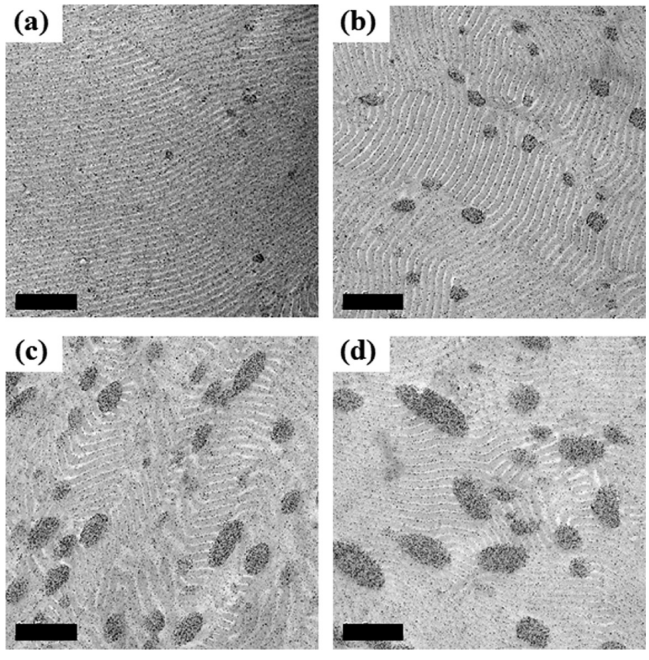

Figure 3. Cross-sectional TEM images of nanocomposites containing (a) ϕ_{NP} = 8.2%, (b) 12.3%, (c) 16.4%, and (d) 20.5% of neutral-ligand Au NPs within PS-*b*-PMMA (M_n = 187 kg/mol). Scale bars are 500 nm.

dx.doi.org/10.1021/am400999z | ACS Appl. Mater. Interfaces 2013, 5, 5659−5666

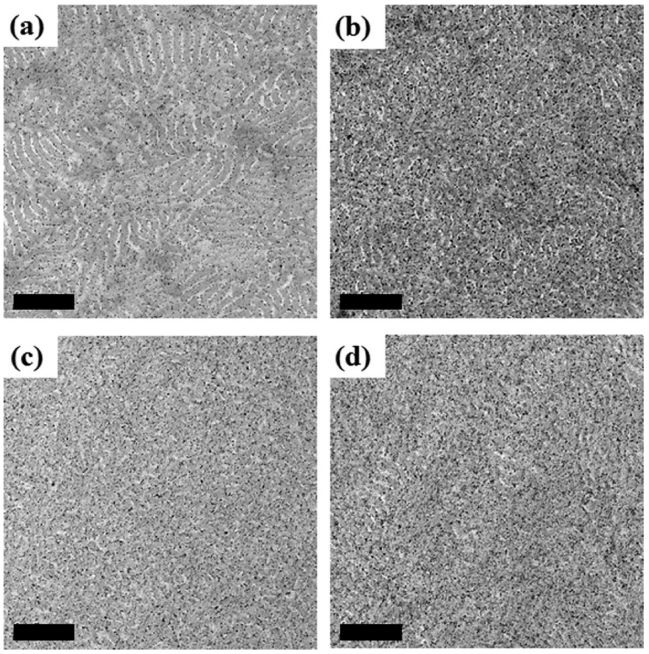

Figure 4. Cross-sectional TEM images of nanocomposites containing (a) ϕ_{NP} = 8.4%, (b) 12.6%, (c) 16.8%, and (d) 21.0% of mixed-ligand Au NPs within PS-*b*-PMMA (M_n = 187 kg/mol). Scale bars are 500 nm.

of NPs loading. However, when the mixed-ligand Au NPs were incorporated, Au NPs were well dispersed within PS-*b*-PMMA block copolymer and the aggregation of Au NPs was not observed. At ϕ_{NP} = 8.4% of mixed-ligand Au NPs loading, it can be seen that lamellae coexist with some disordered structures, indicating that Au NPs start to distort the lamellar interfaces. With further increasing the amount of Au NPs, the lamellar domains completely disappear and the disordered, bicontinuous morphologies were fully developed. However, the individual microdomains of bicontinuous structures were not clearly identified, especially at ϕ_{NP} = 16.8% and 21.0%, presumably because of the low contrast between PS and PMMA blocks and the decrease in the domain size of bicontinuous structures. In addition, to examine the effect of ligand ratios on the formation of bicontinuous structures, we prepared the Au NPs that were coated with various ligand ratios, that is, the feed ratio of ligand-1 as 0.20, 0.30, 0.40, 0.60, 0.70, and 0.80 (see Supporting Information, Table S1). When ϕ_{NP} = 21.0% of these Au NPs were loaded, the bicontinuous structure was developed for Au NPs coated with ligand-1 ratio between 0.4 and 0.6, suggesting that these Au NPs are strongly adsorbed at the PS/PMMA interface (see Supporting Information, Figure S2). However, the macrophase separation was observed for nanocomposites when Au NPs coated with other ratio of ligand-1 (i.e., less than 0.3 or more than 0.7) were added. In this case, it is most likely that these Au NPs depart from the interface and they are segregated within either PS or PMMA domains.

To further investigate the bicontinuous structures, we prepared the thin films of these nanocomposites by adding various amount of mixed-ligand Au NPs into two symmetric

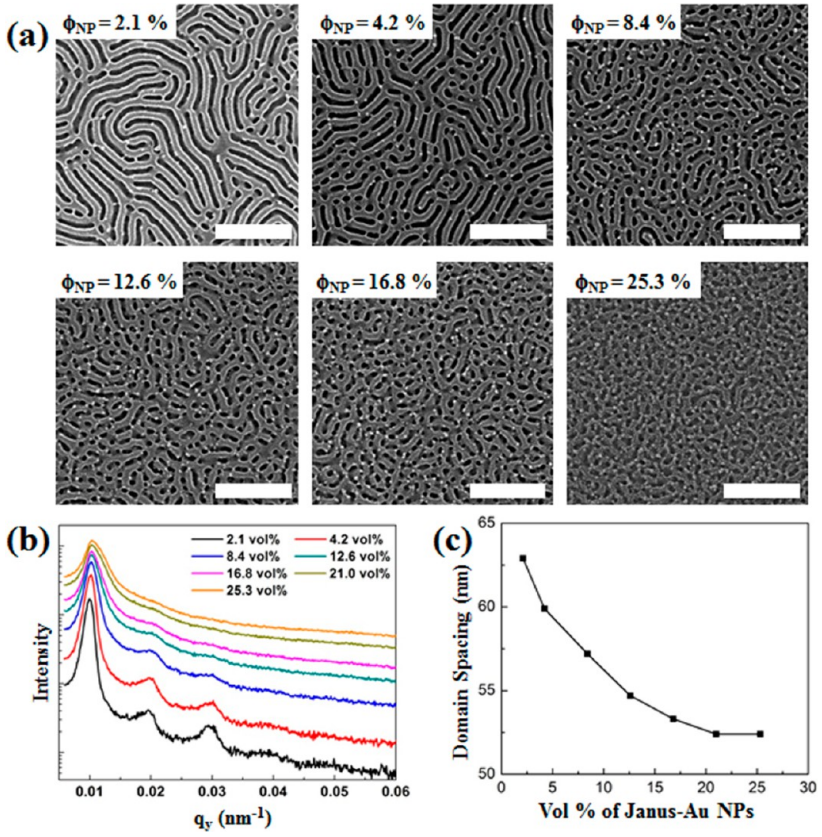

Figure 5. (a) Top view SEM images of nanoporous bicontinuous thin films containing various amount of mixed-ligand Au NPs within PS-*b*-PMMA (130 kg/mol). (b) GISAXS intensity profiles of corresponding thin films in panel a as a function of the scattering vector, *q*. (c) A plot of domain spacing as a function of the weight fraction of mixed-ligand Au NPs. Scale bars in panel a are 40 nm.

dx.doi.org/10.1021/am400999z | ACS Appl. Mater. Interfaces 2013, 5, 5659−5666

PS-*b*-PMMA block copolymers having M_n of 130 kg/mol and 187 kg/mol. The 2.5 wt % toluene solutions of PS-*b*-PMMA were mixed with mixed-ligand Au NPs (ϕ_{NP} was varied from 2.1% to 25.3%) and then the nanocomposite thin films were prepared by spin-casting onto silicon substrates. The film thickness was controlled as ~200 nm. All samples were annealed at 200 °C for two days. To clearly examine the film structures by scanning electron microscopy (SEM), the PMMA microdomains were removed by UV irradiation followed by rinsing with acetic acid, resulting in nanoporous films. From the top-view of SEM images, it is apparent that the thin films containing ϕ_{NP} = 2.1% and 4.2% mixed-ligand Au NPs exhibit the perpendicular orientation of 130 kg/mol and 187 kg/mol PS-*b*-PMMA lamellae (Figure 5a, see also Supporting Information, Figure S3). As we reported previously, the Au NPs that localize at the PS/PMMA interface induce the perpendicular orientation of lamellae, because they move to the substrate to reduce the entropic penalty of the block copolymer chains and thus neutralize the surface of the substrates.[31] With further increasing the mixed-ligand Au NPs loading, the lateral ordering of lamellar patterns becomes short-ranged, resulting in a bicontinuous structures. The formation of bicontinuous structures is also apparent in the cross-sectional SEM images, as the similar disordered structures are fully developed along the vertical direction (see Supporting Information, Figure S4).

While the electron microscopy such as TEM and SEM provides the direct visualization of various morphologies, the information is often limited to very small fraction of samples. On the other hand, the scattering techniques such as small-angle X-ray scattering (SAXS) or small angle neutron scattering (SANS) can collect the quantitative information over relatively large area. In this regards, we quantitatively analyzed the morphological transition from lamellar to bicontinuous structures of nanocomposite thin films by grazing-incidence small-angle X-ray scattering (GISAXS), which was carried out at the 9A beamline at the Pohang Accelerator Laboratory (PAL), Korea. From the in-plane scattering intensity profiles (Figure 5b, see also Supporting Information, Figure S3), the thin films containing ϕ_{NP} = 2.1% and 4.2% of mixed-ligand Au NPs exhibit the sharp first-order reflections and higher order peaks, which corresponds to the well-ordered lamellae having perpendicular orientation. Further increasing the amount of mixed-ligand Au NPs, the intensity of the first-order reflection decreases and the higher order reflections diminish, indicating the transition from well-ordered lamellae to disordered bicontinuous structures. Also, the position of the first-order reflections shift to the higher q with increasing the amount of mixed-ligand Au NPs, as the domain size decreases due to a decrease in interfacial tension, consistent with previous examples reported by Kramer and co-workers.[19,28] In our case, the domain size decreases from 63 to 52 nm (ϕ_{NP} = 2.1% and 25.3% of mixed-ligand Au NPs) for 130 kg/mol PS-*b*-PMMA, and from 94 to 70 nm (ϕ_{NP} = 2.1% and 25.3% of mixed-ligand Au NPs) for 187 kg/mol PS-*b*-PMMA.

From these scattering data, a transition from well-ordered lamellae to the disordered bicontinuous structures can be quantitatively determined. To characterize the phase behaviors of polymer blends in bulk or thin films, the disordered structures such as bicontinuous microemulsion have been analyzed using the Teubner–Strey model[38−40]

$$I(q) \approx \frac{k}{a_2 + c_1 q^2 + c_2 q^4} \quad (1)$$

where $I(q)$ is the scattering intensity as a function of q, the magnitude of the scattering wave vector, and k, a_2, c_1, and c_2 are the associated coefficients. From the fitting of scattering data using the Teubner–Strey model, the amphiphilicity factor, $f_a = c_1/(4a_2c_2)^{1/2}$, can be calculated, which measures the strength of the surfactant in the blends. The ordered lamellar structure corresponds to $f_a = -1$, and the completely disordered structure corresponds to $f_a = +1$.[41] The Teubner–Strey equation was fitted to the GISAXS intensity profiles of nanocomposite films containing mixed-ligand Au NPs within 130 and 187 kg/mol PS-*b*-PMMA block copolymers. The first peaks in the intensity profiles of lamellar and bicontinuous structures were well fitted with the Teubner–Strey equation (see Supporting Information, Figure S5) and f_a was estimated accordingly (Figure 6). As

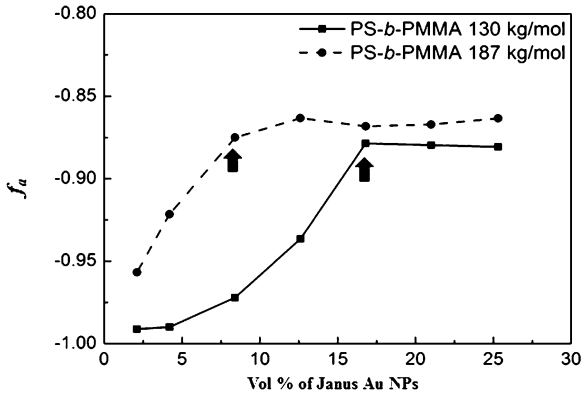

Figure 6. Plot of amphiphilicity factor, f_a, as a function of the volume fraction of mixed-ligand Au NPs. The arrows indicate the onset of transition to the bicontinuous structures.

shown in a plot of f_a as a function of mixed-ligand Au NPs wt %, the value of f_a increases from $f_a \approx -1$ for the well-ordered lamellar structures, and then it levels off to $f_a \approx -0.87$ for 130 kg/mol PS-*b*-PMMA and to $f_a \approx -0.86$ for 187 kg/mol PS-*b*-PMMA. The critical fraction of NPs that induces the transition from lamellar to bicontinuous structures was determined as the onset where f_a values level off, and it corresponds to ϕ_{NP} = 16.8% and 8.4% of mixed-ligand Au NPs for 130 kg/mol and 187 kg/mol PS-*b*-PMMA block copolymer nanocomposites, respectively. In this case, the critical fraction is lower in the 187 kg/mol PS-*b*-PMMA and this observation is consistent with the case of the bicontinuous structures induced by PS grafted Au NPs within PS-*b*-P2VP block copolymers.[19,28] From the strong segregation theory, developed by Ganesan et al., it was shown that the transition from lamellar to bicontinuous structures is driven by a decrease in the bending modulus of the lamellae and also a decrease in the size of lamellar thickness upon NPs loading.[33] Also, they predicted that such effect is more pronounced with a decrease in the size of NPs relative to the lamellar thickness. This can be attributed to the less elastic distortion costs for the polymer and larger surface areas for smaller NPs at the same NPs concentration.

CONCLUSION

In summary, the photocross-linkable polymeric ligands having various compositions of PS and PMMA were synthesized to prepare the thermally stable, shell-cross-linked Au NPs with tuned surface chemistry. The particular focus was on the morphological behaviors between neutral-ligand Au NPs that were coated with ligand-2 having the neutral PS and PMMA

composition and mixed-ligand Au NPs that were modified with equimolar mixtures of ligand-1 (PMMA selective) and ligand-3 (PS selective) upon thermal annealing conditions. At the low content (ϕ_{NP} < 5%) of these Au NPs within PS-*b*-PMMA block copolymer templates, both of them were localized at the PS/PMMA interface. On the other hand, as the amount of Au NPs further increased, the morphological behaviors were completely different in that the neutral-ligand Au NPs exhibited the macrophase separation within PS-*b*-PMMA lamellae whereas the mixed-ligand Au NPs induced the formation of bicontinuous structures without any aggregation of Au NPs. Furthermore, we demonstrated that the nanoporous bicontinuous thin films can be fabricated after removal of PMMA domains. From the GISAXS measurements, it was shown that the domain size of bicontinuous structures decreases with increasing the Au NPs loading, consistent with previous reports on the PS-*b*-P2VP systems. Also, the transition from lamellar to bicontinuous structures was determined by fitting with the Teubner–Strey model. The onset of the bicontinuous structure occurs at the lower fraction of mixed-ligand Au NPs for higher molecular weight of PS-*b*-PMMA as previously predicted by strong segregation theory. We anticipate that our strategy to fabricate the nanoporous bicontinuous structures can be beneficial to various potential applications, such as advanced lithography, nanoscale continuous channels for fuel cells and batteries, photovoltaic films, separation membranes, and so on.

■ ASSOCIATED CONTENT

Ⓢ Supporting Information

TEM images of Au NPs coated with various ligands and the resulting nanocomposites, SEM images of thin film nanocomposties, and fitting data of GISAXS intensity profiles via Teubner–Strey equation. This information is available free of charge via the Internet at http://pubs.acs.org.

■ AUTHOR INFORMATION

Corresponding Author

*E-mail: joona@korea.ac.kr.

Notes

The authors declare no competing financial interest.

■ ACKNOWLEDGMENTS

This work was supported by National Research Foundation of Korea grant funded by the Korea government (MSIP) (No. 2012R1A2A2A01014473) and also by the Human Resources Development Program of KETEP grant (No. 20114010203050) funded by the Korea government Ministry of Trade, Industry and Energy.

■ REFERENCES

(1) Beek, W. J. E.; Wienk, M. M.; Janssen, R. A. J. *Adv. Mater.* **2004**, *16*, 1009–1013.
(2) Liu, J.; Tanaka, T.; Sivula, K.; Alivisatos, A. P.; Fréchet, J. M. J. *J. Am. Chem. Soc.* **2004**, *126*, 6550–6551.
(3) Tseng, R. J.; Huang, J.; Ouyang, J.; Kaner, R. B. *Yang Nano Lett.* **2005**, *5*, 1077–1080.
(4) Bansal, A.; Yang, H.; Li, C.; Cho, K.; Benicewicz, B. C.; Kumar, S. K.; Schadler, L. S. *Nat. Mater.* **2005**, *4*, 693–698.
(5) Tjong, S. C. *Mater. Sci. Eng. R* **2006**, *53*, 73–197.
(6) Rittigstein, P.; Torkelson, J. M. *J. Polym. Sci., Part B: Polym. Phys.* **2006**, *44*, 2935–2943.
(7) Rittigstein, P.; Priestley, R. D.; Broadbelt, L. J.; Torkelson, J. M. *Nat. Mater.* **2007**, *6*, 278–282.
(8) Bockstaller, M. R.; Mickiewicz, R. A.; Thomas, E. L. *Adv. Mater.* **2005**, *17*, 1331–1349.
(9) Kang, D. J.; Kwon, T.; Kim, M. P.; Cho, C. H.; Jung, H.; Bang, J.; Kim, B. J. *ACS Nano* **2011**, *5*, 9017–9027.
(10) Kim, M. P.; Kang, D. J.; Jung, D. W.; Kannan, A. G.; Kim, K. H.; Ku, K. H.; Jang, S. G.; Chae, W. S.; Yi, G. R.; Kim, B. J. *ACS Nano* **2012**, *6*, 2750–2757.
(11) Hostetler, M. J.; Wingate, J. E.; Zhong, C.-J.; Harris, J. E.; Vachet, R. W.; Clark, M. R.; Londono, J. D.; Green, S. J.; Stokes, J. J.; Wignall, G. D.; Glish, G. L.; Porter, M. D.; Evans, N. D.; Murray, R. W. *Langmuir* **1998**, *14*, 17–30.
(12) Bockstaller, M. R.; Lapetnikov, Y.; Margel, S.; Thomas, E. L. *J. Am. Chem. Soc.* **2003**, *125*, 5276–5277.
(13) Shan, J.; Nuopponen, M.; Jiang, H.; Viitala, T.; Kauppinen, E.; Kontturi, K.; Tenhu, H. *Macromolecules* **2005**, *38*, 2918–2926.
(14) Chiu, J. J.; Kim, B. J.; Kramer, E. J.; Pine, D. J. *J. Am. Chem. Soc.* **2005**, *127*, 5036–5037.
(15) Listak, J.; Bockstaller, M. R. *Macromolecules* **2006**, *39*, 5820–5825.
(16) Spontak, R. J.; Shankar, R.; Bowman, M. K.; Krishnan, A. S.; Hamersky, M. W.; Samseth, J.; Bockstaller, M. R.; Rasmussen, K. Ø. *Nano Lett.* **2006**, *6*, 2115–2120.
(17) Kim, B. J.; Bang, J.; Hawker, C. J.; Kramer, E. J. *Macromolecules* **2006**, *39*, 4108–4114.
(18) Kim, B. J.; Bang, J.; Hawker, C. J.; Chiu, J. J.; Pine, D. J.; Jang, S. G.; Yang, S.-M.; Kramer, E. J. *Langmuir* **2007**, *23*, 12693–12703.
(19) Kim, B. J.; Fredrickson, G. H.; Hawker, C. J.; Kramer, E. J. *Langmuir* **2007**, *23*, 7804–7809.
(20) Kim, B. J.; Fredrickson, G. H.; Kramer, E. J. *Macromolecules* **2007**, *41*, 436–447.
(21) Shan, J.; Tenhu, H. *Chem. Commun.* **2007**, 4580–4598.
(22) Li, Q.; He, J.; Glogowski, E.; Li, X.; Wang, J.; Emrick, T.; Russell, T. P. *Adv. Mater.* **2008**, *20*, 1462–1466.
(23) Kim, B. J.; Fredrickson, G. H.; Bang, J.; Hawker, C. J.; Kramer, E. J. *Macromolecules* **2009**, *42*, 6193–6201.
(24) Bain, C. D.; Troughton, E. B.; Tao, Y. T.; Evall, J.; Whitesides, G. M.; Nuzzo, R. G. *J. Am. Chem. Soc.* **1989**, *111*, 321–335.
(25) Dong, H. C.; Zhu, M. Z.; Yoon, J. A.; Gao, H. F.; Jin, R. C.; Matyjaszewski, K. *J. Am. Chem. Soc.* **2008**, *130*, 12852–12853.
(26) Yoo, M.; Kim, S.; Lim, J.; Kramer, E. J.; Hawker, C. J.; Kim, B. J.; Bang, J. *Macromolecules* **2010**, *43*, 3570–3575.
(27) Jang, S. G.; Khan, A.; Dimitriou, M. D.; Kim, B. J.; Lynd, N. A.; Kramer, E. J.; Hawker, C. J. *Soft Matter* **2011**, *7*, 6255–6263.
(28) Jang, S. G.; Kim, B. J.; Hawker, C. J.; Kramer, E. J. *Macromolecules* **2011**, *44*, 9366–9373.
(29) Lim, J.; Yang, H.; Paek, K.; Cho, C. H.; Kim, S.; Bang, J.; Kim, B. J. *J. Polym. Sci., Part A: Polym. Chem.* **2011**, *49*, 3464–3474.
(30) Kim, B. J.; Chiu, J. J.; Yi, G. R.; Pine, D. J.; Kramer, E. J. *Adv. Mater.* **2005**, *17*, 2618–2622.
(31) Yoo, M.; Kim, S.; Jang, S. G.; Choi, S.-H.; Yang, H.; Kramer, E. J.; Lee, W. B.; Kim, B. J.; Bang, J. *Macromolecules* **2011**, *44*, 9356–9365.
(32) Noro, A.; Higuchi, K.; Sageshima, Y.; Matsushita, Y. *Macromolecules* **2012**, *45*, 8013–8020.
(33) Pryamitsyn, V.; Ganesan, V. *Macromolecules* **2006**, *39*, 8499–8510.
(34) Schreiber, F. *Prog. Surf. Sci.* **2000**, *65*, 151–256.
(35) Zhao, B.; Zhu, L. *Macromolecules* **2009**, *42*, 9369–9383.
(36) Liu, X.; Yu, M.; Kim, H.; Mameli, M.; Stellacci, F. *Nat. Commun.* **2012**, 3 DOI: 10.1038/ncomms2155.
(37) Futterer, T.; Vliegenthart, G. A.; Lang, P. R. *Macromolecules* **2004**, *37*, 8407–8413.
(38) Teubner, M.; Strey, R. *J. Chem. Phys.* **1987**, *87*, 3195–3200.
(39) Liu, G.; Stoykovich, M. P.; Ji, S.; Stuen, K. O.; Craig, G. S. W.; Nealey, P. F. *Macromolecules* **2009**, *42*, 3063–3072.
(40) Zhou, N.; Lodge, T. P.; Bates, F. S. *J. Phys. Chem. B* **2006**, *110*, 3979–3989.
(41) Schubert, K. V.; Strey, R.; Kline, S. R.; Kaler, E. W. *J. Chem. Phys.* **1994**, *101*, 5343–5355.